

Christopher D. Karstens^{1*}, Timothy M. Samaras², William A. Gallus, Jr.¹,
Catherine A. Finley³, Bruce D. Lee³

¹ Iowa State University, Ames, IA.

² National Technical Systems, Littleton, CO.

³ Wind Logics Inc., Grand Rapids, MN.

1. INTRODUCTION

The near-ground region of a tornado (i.e., corner flow region) experiences significant changes in structure (i.e., single-, two-, and two-cell with multiple vortices) and intensity (i.e., peak pressure drop, maximum wind speed) during its lifetime. Given the unpredictability of tornado occurrence and difficulty in obtaining observations, very little documentation outside of modeling studies exists relating these two components of tornado evolution (e.g. Kosiba et al. 2008; Karstens et al. 2010).

Changes in intensity are often evidenced by spatial variations in the degree(s) of damage caused by the tornado. Tornado intensity has traditionally been determined from damage using the Fujita or Enhanced Fujita Scales. However, known complexities in estimating wind speeds from damage limit the value of these intensity determinations (Doswell 2009). In some instances, video documentation of the tornado may exist, and on rare occasions, aerial photographs of scour marks, in addition to damage, produced by the tornado are available. Although videos and photos offer a limited means of quantitatively estimating intensity-related information (e.g., Golden and Purcell 1977), their qualitative value in deciphering information, such as vortex structure, can be beneficial.

To characterize the flow governing tornado vortex structure, laboratory and numerical studies have employed the non-dimensionalized parameter swirl ratio. Swirl ratio can take on many forms, but traditionally it is defined as

$$S = \frac{r_0 \Gamma}{2Qh} = \frac{\Gamma}{2Qa}, \quad (1)$$

where r_0 is the radius of the updraft; Γ , the circulation at r_0 (i.e., angular momentum); Q , the volume flow rate per axial length or the volume flow rate across the updraft; h , the inflow depth; and a , the internal aspect ratio: h/r_0 (e.g., Church et al. 1979; Snow et al. 1980). Relatively low values of the swirl ratio have been associated with single-cell vortices, with a progression toward two-cell and two-cell with multiple vortices as swirl ratio increases. However, the application of the swirl ratio to the unconfined and asymmetric flow near a tornado is problematic.

* Corresponding author address: Christopher D. Karstens, Iowa State Univ., Dept. of Geol. and Atm. Sciences, Ames, IA; email: karstens.chris@gmail.com.

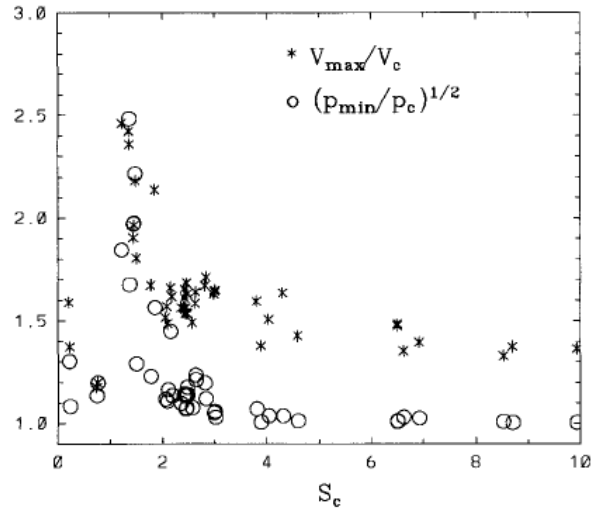


Figure 1. Non-dimensional ratios representative of peak vortex intensity as a function of the local corner flow swirl ratio (S_c). Peak intensity occurs when S_c is near 1.2. Figure is from Lewellen et al. (2000).

In addition to the difficulty of applying swirl ratio to a tornado, Lewellen et al. (2000) found that slight adjustments in the inflow boundary conditions, while holding the swirl ratio and other parameters constant, can have a profound impact on vortex structure. Thus, a relationship cannot be established between the traditional swirl ratio and vortex structure in every case. Consequently, they proposed the implementation of a more robust expression for the swirl ratio, called a local corner flow swirl ratio, defined as

$$S_c = \frac{r_c \Gamma_\infty^2}{Y}, \quad (2)$$

where r_c is the core radius in the quasi-cylindrical symmetric region of the vortex above the surface; Γ_∞/V_c , where V_c is the maximum tangential velocity in the quasi-cylindrical region, Γ_∞ is the angular momentum flowing into the domain, and Y is the total depleted angular momentum flux flowing from the surface into the corner flow region. Lewellen et al. show that a maximum in intensity occurs for S_c around 1.2, corresponding to a low-swirl corner flow structure (Fig. 1). Importantly, they suggest that any mechanism responsible for transitioning S_c closer (further) to (from) a value of 1.2 will lead to vortex intensification (decay)

near the surface. Considering a tornado with $S_c > 1.2$ initially, intensification results when low angular momentum flow far from the tornado centroid is eventually ingested into the tornado. They accomplished this by increasing surface roughness, tornado translation speed, or introducing low angular momentum flow outside or below the broad-scale circulation. Lewellen et al. (2000) notably point out that the later of these may be of critical importance to this aspect of research.

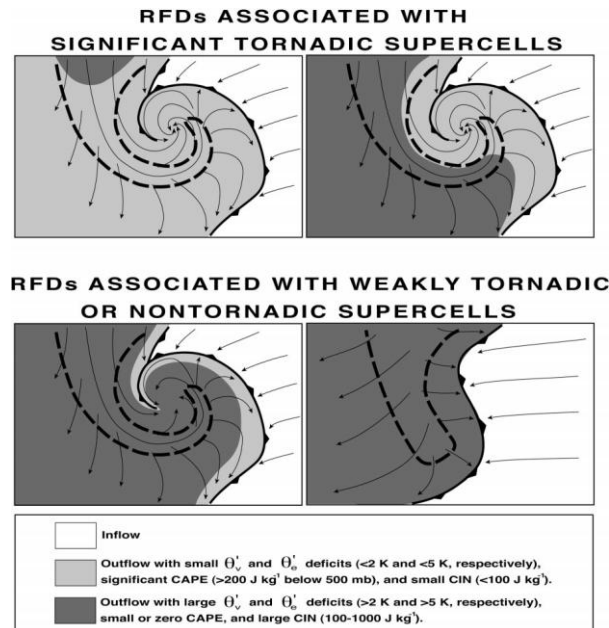


Figure 2. Schematic diagram illustrating the thermodynamic characteristics of RFDs associated with significantly tornadic, and weakly tornadic or nontornadic supercells. Figure is from Markowski et al. (2002).

In the past decade or so, studies have utilized measurements taken in the RFD of supercells, using a mobile mesonet, to characterize the relationship between Rear-Flank Downdraft (RFD) thermodynamics and tornado occurrence (e.g., Markowski et al. 2002; Grzych et al. 2007). These studies found that RFDs associated with significantly tornadic events are characterized by low θ'_e and θ'_v deficits (Fig. 2). However, an important shortcoming to these studies is a lack of spatial coverage within a 1 km radial distance from the tornado. Lee et al. (2010a) make a first attempt at documenting the thermodynamics in this region, and find a consistency in their θ'_e and θ'_v deficits with the aforementioned studies.

In an effort to better understand the thermodynamics of parcels closely bounding and moving toward the tornado, this research was designed to examine the directional orientation and thermodynamic properties of air parcels in the near-ground, near-tornado (1 km) region. Is there a

preference of air with low θ'_e and/or θ'_v deficits to move toward the tornado, and are certain quadrants favored for providing near-tornado inflow? This study uses two of five available cases collected by the Tactical Weather Sampling in/near Tornadoes Experiment (TWISTEX) from 2008 to 2010. The data are analyzed in a tornado-relative framework, with velocities decomposed into their radial and tangential components. In addition to the kinematic and thermodynamic analysis, evolution of each tornado's visually-inferred structure and intensity, and subjectively-determined translation speed, direction, and path width are documented.

Methodologies for the instrumentation, data collection and conversion, and post-processing techniques are discussed in section two. Cases used for the analysis and their results are discussed in section three. Preliminary conclusions are outlined in section four and we close in section five with our plans and suggestions for future research.

2. METHODOLOGY

2.1 Instrumentation and Data Collection

The instruments used in this study are part of a diverse collection of instruments that comprise a mobile mesonet station (Straka et al. 1996; Grzych et al. 2007). Data from four (three pre-2009) mobile mesonet stations were available. The sensors were mounted at 3 m AGL on three stations (M1, M2, and M3) and at 3.5 m AGL on the station added in 2009 (MT). A sampling frequency of 1 Hz (0.5 Hz pre-2009) was used.

The mesonet stations from the TWISTEX and ANSWERS projects have been primarily used to study the kinematic and thermodynamic character of the RFD and the internal RFD surges that occur near a tornado (e.g., Grzych et al. 2007; Lee et al. 2010). To satisfy the RFD-related objectives, these stations maintain a tornado-relative position of 1 - 1.5 km relative to each other, with the closest stations sometimes sampling within 1 km of the tornado edge. In this study, we make use of the mesonet station data to analyze the behavior of the wind in close proximity (i.e., < 1 km to the tornado edge), but not inside, the tornado.

2.2 Spatial Conversion of Observations

In this study, we considered two types of spatial conversion of the observations. The first type is the traditional time-to-space conversion, which uses a mean translation vector that is representative of the feature in question. An overview of this conversion is given in Markowski et al. (2002). In essence, one assumes that all features relevant to the phenomena in question are in a pseudo steady-state during the period of analysis. In the case of spatially converting observations near a tornado, one assumes a mean tornado translation vector over what typically equates to a two to five minute period.

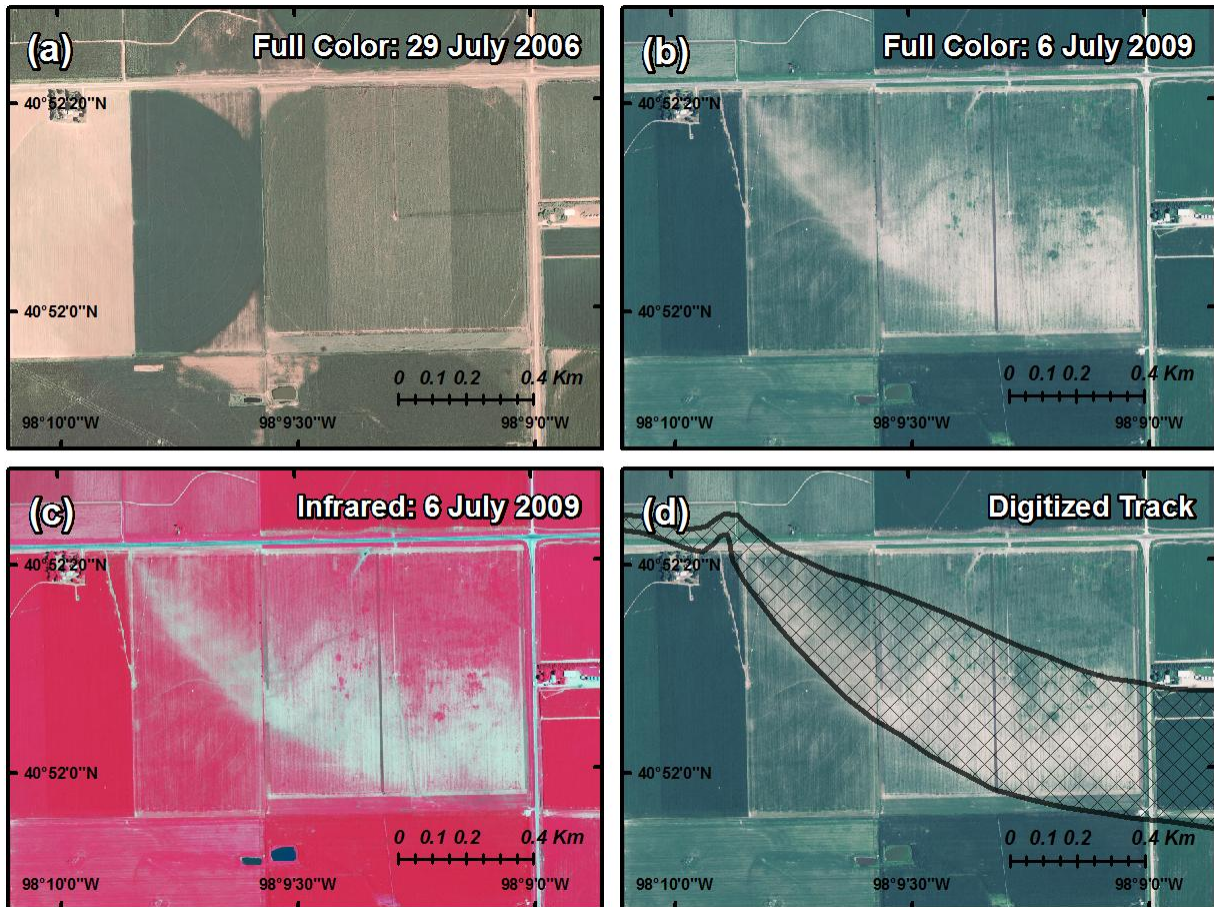


Figure 3. Illustrated process of digitizing a tornado track using aerial orthophotos by utilization of a) a full-color photo taken before the tornado occurred, and b) a full-color photo and c) an infrared photo taken shortly after the event. The resulting track is shown in panel d.

Thus, any deviation of the vortex translation relative to the mean during this period is not accounted for.

The second type of spatial conversion considered is a feature-relative conversion. To conduct this type of conversion, one must know the position of both the phenomena in question and the features relative to it, concurrently. In the example of converting observations near a tornado, one must simultaneously know the location of the observations and the tornado centroid. Mobile mesonet and in situ observations are typically acquired at a rate ranging from 0.5 to 10+ Hz and are geo-located using GPS. As addressed in Markowski et al. (2002), pinpointing the temporally dependent location of the tornado centroid is a difficult task without four-dimensional kinematic fields. However, in section 2.3 we offer an alternative method to acquire the temporally-dependent tornado centroid position, thus allowing for a feature-relative conversion.

We believe using the feature-relative conversion is more suitable for this study. Our intention is to

investigate the relationship between peripheral near-ground winds and tornado structure and intensity. As previously described, these features may depend on spatially- and temporally-dependant parcel characteristics feeding into the tornado and near-tornado environment. Thus, making accurate decompositions of the velocities into their radial and tangential components is essential.

The question of an appropriate scale to use must also be addressed. At what distance are air parcels most likely making their way into the tornado? We believe the answer is a function of radial distance from the edge of the tornado at a given time, and, to a lesser extent, how radial the flow is at a given time and distance from the tornado edge. For the purposes of this study, we only consider observations that were obtained within 1 km of the edge of the tornado. Time-series plots were created from these close-proximity measurements and are presented in section 3.

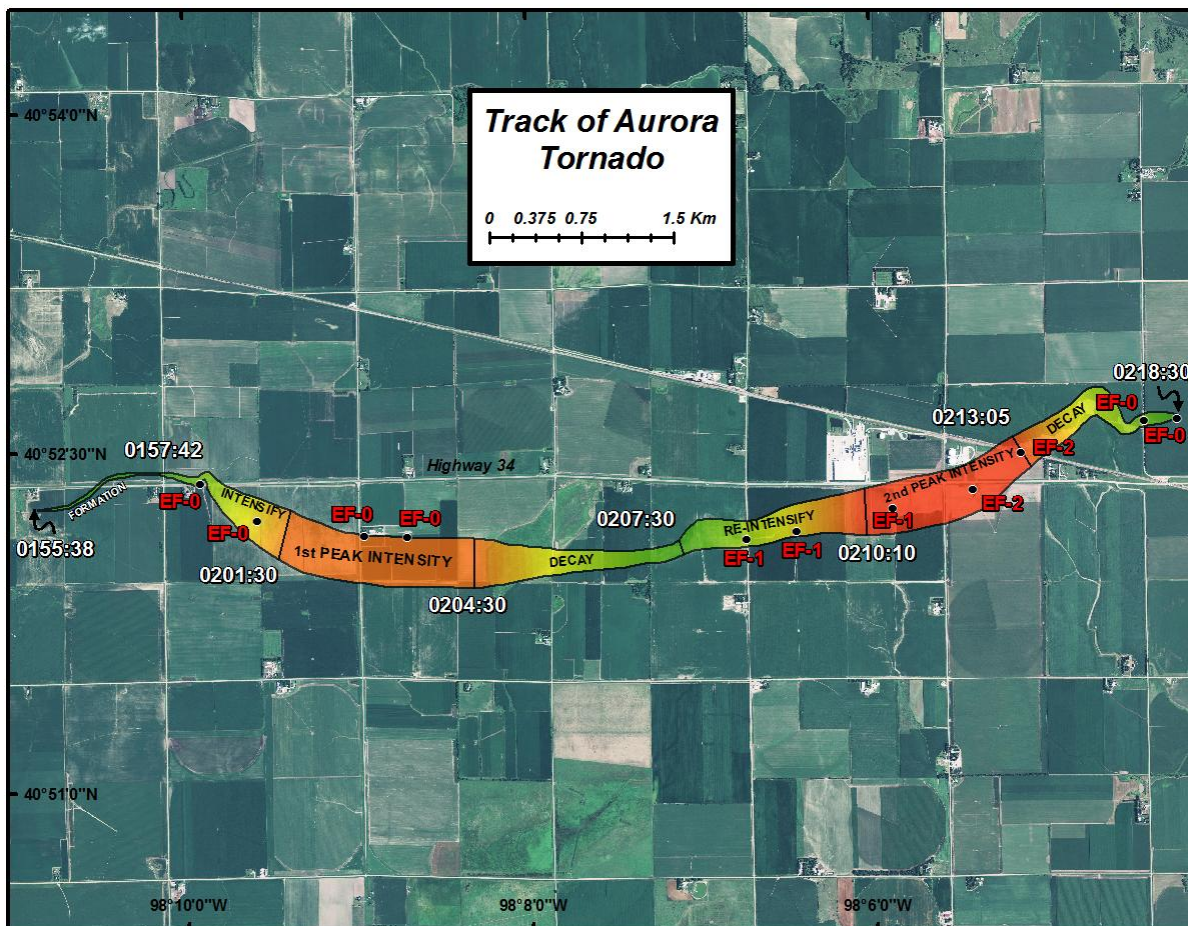


Figure 4. Track of the Aurora tornado. Shaded areas indicate transitions in tornado intensity. Times corresponding to changes in tornado intensity shown in white. NWS damage indicators marked with black dots.

2.3 Post-Processing

The mesonet datasets were quality-controlled for spurious meteorological readings and vehicle headings. Biases were removed by making use of inter-comparisons between mesonet stations for extensive periods when the caravan was in relatively uniform meteorological conditions and predominantly in transit. Velocity data were removed in a similar manner as that employed by Markowski et al. (2002) and Grzych et al. (2007), owing to inaccuracies in the anemometry during significant vehicle accelerations. A 3-second centered averaging was applied to the wind measurements.

Two methods were used to estimate the temporally-dependent location of the tornado centroid. In one method, we used a combination of synchronized video from the mesonet teams and aerial orthophotos to digitize the tornado's centroid and width at the base, similar to the method used in Wakimoto et al. (2003), in 10 s intervals. Landmarks, such as trees, buildings, etc., identifiable in both the video and orthophotos were used to estimate the tornado centroid azimuth relative to each mesonet station's position when possible. This allowed for bearing-bearing, triple bearing, and

quadruple bearing offsets to be computed when two, three, and four cameras were capturing the tornado, respectively.

In the other method, we used full-color aerial orthophoto imagery, taken both before (Fig. 3a) and shortly after (Fig. 3b) the event (when possible), to digitize areas of scouring produced by the tornado (Fig. 3d). In addition to using full-color photos, infrared orthophotos were also used in digitizing the track when possible (Fig 3c). Infrared images show stress to plants and are typically utilized to digitize areas absent of chlorophyll (e.g., small ponds, bottom center of Figs. 3b and 3c).

A linear interpolation was applied to the tornado centroid positions to provide position, speed, heading, and width information for every second of the tornado's life. This information was used to make a feature-relative conversion of the observations, as previously discussed. Wind measurements were decomposed into their radial and tangential components for directional analysis. To represent the ratio of these two wind components, we define a proxy inflow swirl ratio (S_i), expressed as,

$$S_i = \frac{V_{\tan}}{V_{\text{rad}}} \quad (3)$$

Values between $0 < S_i < 1$ are considered radial, and $S_i > 1$ are considered tangential. When $S_i < 0$, negative radial components are present. Extreme values of S_i (i.e., $S_i > 7$ and $S_i < -7$) were excluded from the analysis. Additionally, the instantaneous tornado translation vector was subtracted from the wind measurements. Thus, the analyzed winds presented in this study are considered tornado-relative winds.

3. CASES AND PRELIMINARY RESULTS

3.1 17 June 2009

The storm of interest to this study, hereafter referred to as the Aurora storm, produced four tornadoes in total. Two weak tornadoes occurred north of Gibbon, NE, rated EF-1 and EF-0, and one tornado occurred on the south side of Grand Island, NE, rated EF-0 (NWS 2010a; NWS 2010b). The final, main tornado episode, #4, occurred west of Aurora, NE and was rated EF-2 (NWS 2010c). We discuss measurements taken from tornado episode #4, hereafter referred to as the Aurora tornado (Fig. 4). Analysis of the broader RFD characteristics from tornado episode #3 and the Aurora tornado may be found in Lee et al. (2010b).

Tornadogenesis occurred at approximately 0155:38 UTC. The tornado ended at approximately 0218:30, lasting nearly 23 minutes. During this period of time, the tornado traveled approximately 10.1 km and scoured 2.4 km² of land (Fig. 4). The tornado underwent several changes in structure and intensity during its lifetime. Periods of transition (Fig. 4, gradient colors) and quasi-steadiness (Fig. 4, solid colors) in intensity were identified from video documentation. These intensity periods are labeled on figures 5, 6, 7 and 8, and are discussed in the following sub-sections.

3.1.1 Formation: 0155:38 - 0159:30

From the time of formation until about 0159:30, the tornado visually was a narrow condensation funnel that was positioned above a multiple-vortex ground circulation (Fig. 6a). The circulation began south of Highway 34, traveling northeast and crossing the highway, before turning toward the east, maintaining a width between ~25 and ~50 m (Figs. 5b and 5c). The translation speed of the tornado notably decreased during this time period (Fig. 5a). Of the four mobile mesonet stations available, only one (MT) was within 1 km of the edge of the tornado at any time during this period. This was also true for the remaining periods in this case, thus, only measurements from MT are discussed.

At tornadogenesis, MT was positioned northeast of the tornado, within about 250 m of its edge (Figs. 7 and 8). The flow here was largely tangential ($S_i > 4$). As the

tornado crossed Highway 34 to the east of MT, the measured flow transitioned from being tangential to being directed radially outward from the tornado ($S_i < 0$). This is indicative of a small RFD surge. Further details of this surge may be found in Lee et al. (2010b). Interestingly, even though the tornado was forming, the measurements that were made very close to the tornado, in quadrants I, IV and III, did not show large radial components. It is important to note that intensification of the tornado occurred several minutes after these close proximity measurements were made.

Thermodynamically, the environment near the tornado was quite complex. Large θ_e (-10 to -12 K) and small θ_v (-1 to -2 K) deficits were observed close to the tornado (Fig. 7). Within the RFD surge, θ_e deficits were slightly warmer (-8 to -10 K) and θ_v deficits were slightly cooler (-2 to -3 K). Although the θ_v deficits are consistent with the findings of Markowski et al. (2002) and others for significantly tornadic events, the θ_e deficits are more consistent with weakly tornadic or nontornadic events.

As MT crossed out of an internal RFD outflow surge boundary at 0157:30, farther west-southwest of the tornado, the flow showed more of an inward radial component ($0 < S_i < 1$; Figs. 7 and 8). Concurrently, as MT's distance from the edge of the tornado increased, the θ_e deficits became much larger (-16 to -20 K) through the end of the period. Note, these measurements were made just before the tornado began to intensify, but relatively far away. Although these measurements were confined primarily near the boundary of quadrants III and IV and outside of the RFD surge, it is interesting that the flow was nearly completely radial just prior to the tornado's intensification.

3.1.2 Intensification: 0159:30 - 0201:30

From 0159:30 to 0201:30, the tornado underwent rapid intensification. This was evidenced by a dramatic change in width, from ~50 m to ~400 m during this time (Figs. 5c, 6b and 6c). The translation speed of the tornado increased with time, from ~4 to ~10 m s⁻¹ (Fig. 5a). A change in vortex structure was also apparent, as the tornado transitioned from a multiple-vortex configuration to primarily two-cell structure.

Interestingly, a sinusoidal pattern in the translation direction is apparent in figure 5b, noted at the beginning of this intensification period. This feature is coincident with a minor decrease in translation speed, and subsequent widening of the tornado. Prior studies have documented a similar sinusoidal pattern in the tornado track, including a cusplike pattern (e.g. Wakimoto et al. 2003). Brown and Knupp (1980) speculate this type of pattern is the result of the tornado being a single vortex in a multiple-vortex mesocyclone (e.g. Wurman and Kosiba 2008). Visually, at the beginning of this period, the tornado appeared to be located on the northeastern edge of the mesocyclone. Given the eastward movement of the mesocyclone, the Brown and Knupp explanation could be plausible.

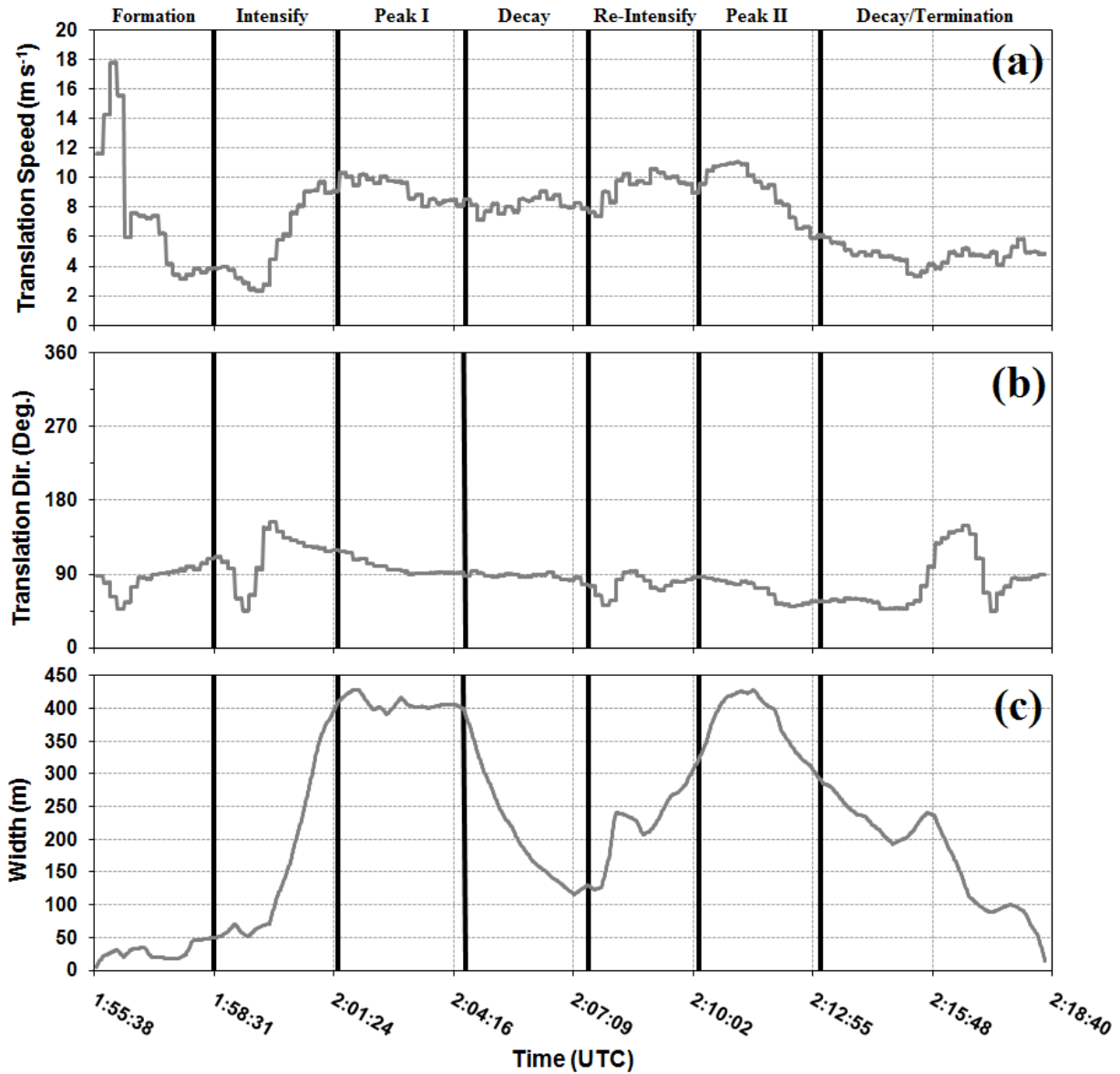


Figure 5. Temporal evolution of the Aurora tornado's a) translation speed, b) translation direction, and c) width. Vertical black bars correspond to the intensity periods (labeled at the top) identified in Fig. 4.

At the beginning of this period, MT began driving east on Highway 34 toward the tornado and sampling the quadrant III and IV boundary region (Figs. 7 and 8). As MT crossed back through the internal RFD outflow surge boundary, the flow rapidly transitioned from largely radial to more tangential. Within the near-tornado RFD, θ_e and θ_v deficits were again in the -10 to -12 K and -2 to -3 K range, respectively. MT drove to within 200 m of the edge of the tornado, before coming to a stop west-northwest of the tornado. Winds at this ~200 m range showed a much larger radial component ($0 < S_i < 1$), compared to winds beyond a radial distance of ~300 m, which showed more of tangential component.

Evidence of large radial wind components in very close proximity to the tornado during the intensification stage suggests the tornado was being driven toward a lower corner flow swirl ratio, supporting the findings of Lewellen et al. (2000). This is supported by visual evidence of the tornado transitioning toward a two-cell structure, and by an increase in the tornado's translation speed. As discussed previously, the large θ_e deficits measured during this period do not coincide with findings from prior RFD studies, even though the θ_v deficits are more consistent with past studies for RFDs associated with tornadoes.



Figure 6. Video screenshots of the Aurora tornado taken at the beginning of the a) formation, b) intensification, c) peak intensity I, d) decay, e) re-intensification, f) peak intensity II, and g) decay/termination periods during the tornado's life. Panel h) shows the Aurora tornado near termination. All times are in UTC.

3.1.3 Peak Intensity I: 0201:30 - 0204:30

The Aurora tornado reached its first of two peak intensities at 0201:30, lasting until 0204:30. The tornado appeared to maintain a two-cell structure, with no apparent multiple-vortices during this period of time. The tornado also remained quite wide (~400 m; Fig. 5c)

as it traveled at a near-constant speed, with the condensation funnel positioned above the intense ground circulation (Figs. 6c and 6d). The tornado continued traveling in an arc, with a southeasterly heading initially that transitioned more toward the east with time. Another feature of interest was the evolution of a dust plume that originated nearly due south of the

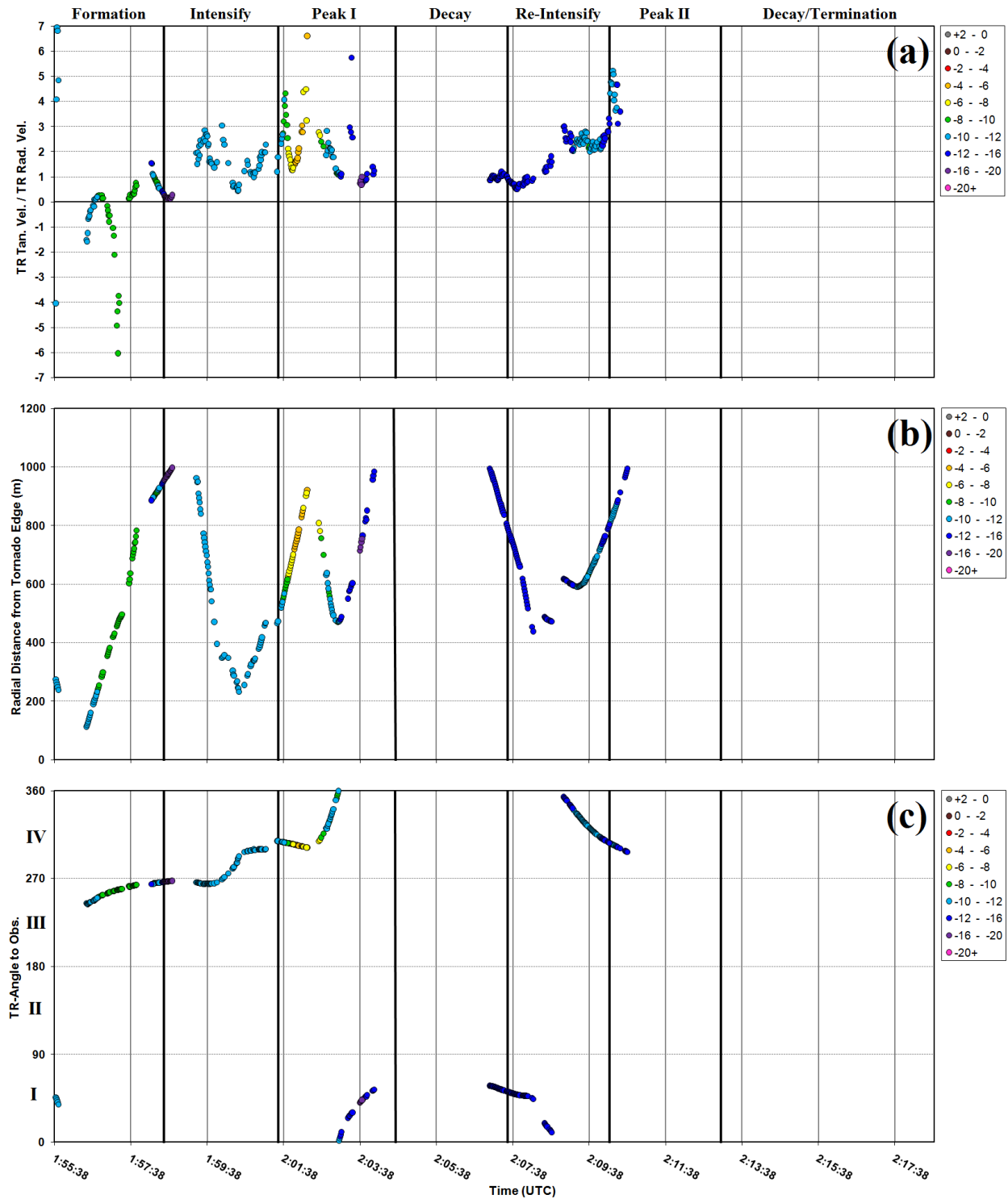


Figure 7. Analysis of θ_e' (colored dots) superimposed on the time series analyses of a) S_i , b) radial distance from the tornado edge, and c) tornado-relative angle of the observations for the Aurora tornado. Intensity periods labeled at the top and separated by the vertical black bars. Traditional RFD quadrants are labeled on panel c.

tornado at the beginning of the period. With time, this plume of dust appeared to wrap around the eastern edge and into the tornado as the tornado widened. The plume was associated with the leading edge of an

internal RFD surge measured by MT early in the tornado's life. Further discussion of this plume may be found in Lee et al. (2010b).

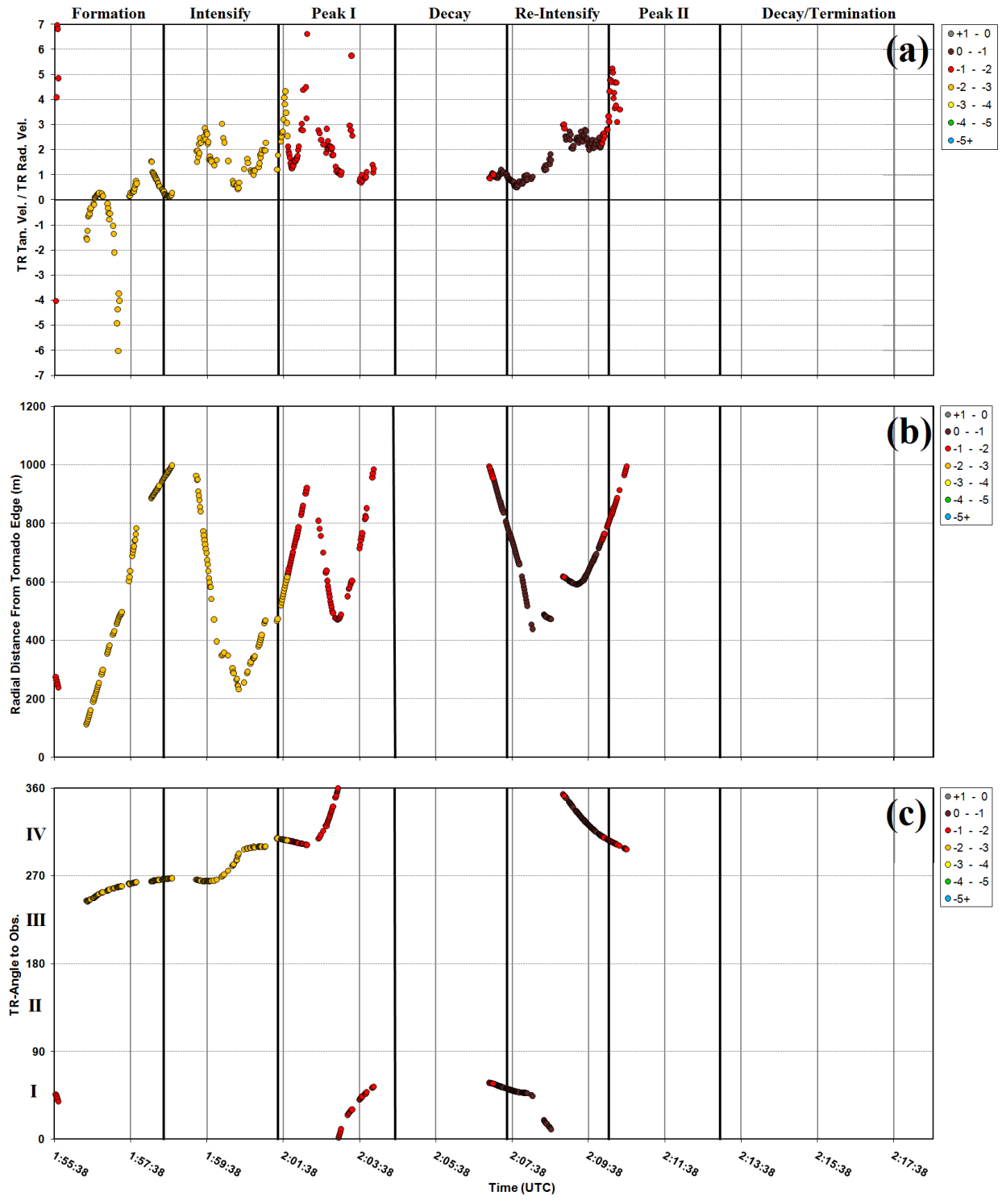


Figure 8. As in Fig. 7, except for θ_v' .

During the tornado's first peak intensity period, MT was positioned west-northwest of the tornado. Approximately half-way through the period, MT began driving east on Highway 34, moving north and eventually east-northeast of the tornado by 0204:30. Winds during this time were primarily tangential to the

tornado, although near the end of the period, low values of S_i ($0 < S_i < 1$) were observed (Figs. 7 and 8). MT appears to have passed through two θ_e' gradients, one with smaller than previously measured deficits (-4 to -6 K) at the beginning (west-northwest of the tornado), and one with very large deficits (-16 to -20 K) near the end of

the period (east-northeast of the tornado). These measurements show that a rapid change in the air mass occurred west-northwest of the tornado, with a steady progression toward lower θ_e deficits. Additionally, some of the largest θ_e deficits were observed east-northeast of the tornado, just prior to the decay period.

3.1.4 Decay: 0204:30 - 0207:30

At 0204:30, the tornado began to gradually decay. This was evidenced by a decrease in the ground circulation's intensity and width with time. Much of the lofted debris began to settle out, and the condensation funnel aloft nearly disappeared (Fig. 6e). The tornado maintained an easterly course at $\sim 8 \text{ m s}^{-1}$. Visually, the tornado appeared to change from a two-cell structure to a two-cell structure with multiple vortices.

During this period, MT was positioned east-northeast of the tornado, near Highway 34. Observations meeting our scale criteria were obtained as the tornado drew closer to MT, near the end of this period. These observations were approximately 800 to 1000 m from the tornado edge.

The flow was highly radial at this time (Figs. 7 and 8). Given that a re-intensification was observed shortly after these measurements were made, and that the tornado showed a relatively high swirl corner flow structure, the notion that the introduction of radial flow at large radii can potentially lead to rapid tornado intensification is supported by these measurements. However, the thermodynamic signal is somewhat contradictory. Since there are similarities in the parcel thermodynamics between this period as the next, discussion on the thermodynamic characteristics of the flow may be found in the next section.

3.1.5 Re-Intensification: 0207:30 - 0210:10

At 0207:30, the tornado appeared to rapidly intensify once again. This was again evidenced by an intensification in the ground circulation and widening of the tornado, and the reappearance of a condensation funnel (Figs. 5c and 6f). The tornado translation speed also increased slightly to $\sim 10 \text{ m s}^{-1}$ (Fig. 5a). Additionally, the structure of the tornado visually appeared to change from a two-cell structure with multiple vortices to a single cell structure during this short period, suggestive of a transition toward a lower corner flow swirl ratio. One HITPR probe was deployed east-northeast of the tornado by MT. Analysis of these measurements will be presented at a later time.

Once again, a sinusoidal pattern in the translation direction is evident at the beginning of this period (Fig. 5b). Visually, the pattern looks similar to the cusplike feature mentioned previously (Fig. 4). Both of these sinusoidal patterns occurred shortly before tornado intensification. At this time, we feel it is premature to make any suggestions or possible linkages between this apparent sinusoidal or cusplike pattern and tornado intensity, however, we do find it interesting that this type

of pattern occurred twice with the same tornado, just prior to intensification.

A continuation of highly radial flow was observed through the first half of this period, primarily confined to quadrant I (Figs. 7 and 8). Again, this evidence is supportive of the findings of Lewellen et al. (2000), however the θ_e deficits remained quite large (-12 to -16 K). Surprisingly small θ_v deficits observed in this quadrant (0 to -1 K). As the tornado passed by to the south, MT observed slightly smaller θ_e deficits (-10 to -12 K) north-northwest of the tornado, but these are still fairly large for a significantly tornadic event.

3.1.6 Peak Intensity II: 0210:10 - 0213:05

At 0210:10, the tornado appeared to reach its second of two peak intensities. The ground circulation visually appeared more intense than during the first peak intensity period (Figs. 6f and 6g), thus we believe the tornado reached its peak intensity at this time. The tornado appeared to maintain a low-swirl single-cell structure, or perhaps a medium-swirl two-cell structure throughout this period. Midway through this period, the tornado once again reached a peak width just over 400 m, as it traveled east-northeast at $\sim 11 \text{ m s}^{-1}$ (Fig. 5). As the tornado approached Highway 34, it struck a farmstead and produced EF-2 damage. A short while later, near the end of this period, the tornado crossed a railroad track where, coincidentally, a number of railcars were parked. These railcars were rolled off the track, and they were assigned an EF-2 rating as well. These two damage indicators received the highest EF-scale rating compared to all other structures damaged along the tornado track, suggesting the tornado was indeed at peak intensity at this time. However, it is important to note that the tornado occurred in open terrain (free of well-built damage indicators) for much of its life.

Limited measurements are available for this period. These measurements were obtained northwest of the tornado by MT, as the tornado continued to move east of their mesonet station. The winds continued to show a progression toward more of a tangential orientation, with θ_e deficits remaining in the -10 to -12 K range (Figs. 7 and 8). The θ_v deficits slightly decreased at this time, back into the -1 to -2 K range.

3.1.7 Decay/Termination: 0213:05 - 0218:30

After crossing the railroad tracks, the tornado began steadily decreasing in intensity. Visually, the ground circulation became very wide and not very intense (Fig. 6h). Orthophoto evidence suggests the most intense part of the tornado was contracting with time. A remnant dust cloud gave the tornado a wide appearance. Visually, the tornado appeared to steadily transition toward a two-cell structure. The estimated time of termination was at 0218:30, based on video documentation. Interestingly, occupants in M2 and M3 observed a weak, possibly

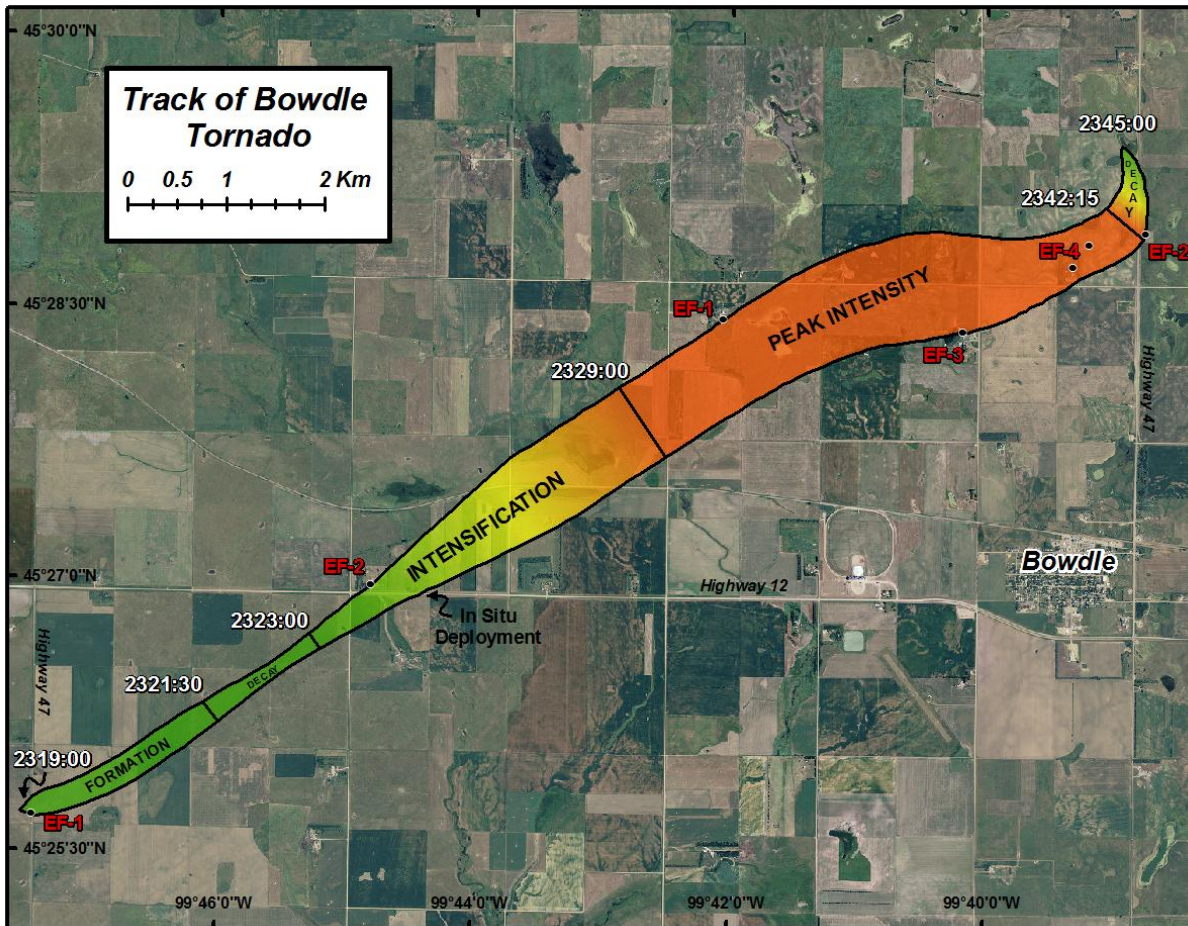


Figure 9. As in Fig. 4, except for the Bowdle tornado.

anticyclonic tornado located southeast of the dying Aurora tornado. Further analysis of this tornado may be found in Lee et al. (2010b).

Considering that the Aurora tornado was decreasing in intensity during this period, and that a possible new tornado was forming concurrently, no close proximity measurements were made during this time period.

3.2 22 May 2010

The storm of interest to this study, hereafter referred to as the Bowdle storm, produced perhaps as many as seven tornadoes (ABR NWS 2010, personal communication). We discuss measurements taken from tornado episode #2, hereafter referred to as the Bowdle tornado. Analysis of the broader RFD characteristics from tornado episode #1 and the Bowdle tornado may be found in Finley et al. (2010).

The Bowdle tornado formed at approximately 2319:00 UTC and ended at approximately 2345:00 UTC, lasting about 26 minutes (Fig. 9). During this period of time, the tornado traveled roughly 13.9 km and scoured 8.1 km² of land. Similar to the previous case, periods of transition (Fig. 9, gradient colors) and quasi-

steadiness (Fig. 9, solid colors) in intensity were identified from video documentation. These intensity periods are labeled on Figures 10, 11, 12, and 13.

3.2.1 Formation: 2319:00 - 2321:30

Genesis of the Bowdle tornado occurred just a few 10s of meters west of Highway 47, southwest of Bowdle, at approximately 2319:00. At this time, the parent supercell was cycling, with tornado episode #1 ending a just a few seconds prior to tornadogenesis. Video documentation of tornadogenesis suggests the Bowdle tornado began as a secondary vortex within the larger mesocyclonic circulation (Fig. 11a). As the tornado formed, it rapidly intensified and crossed Highway 47, traveling northeast. The funnel was fully condensed to the ground, and the ground circulation, estimated at 300 m in diameter (Fig. 10c), was rather intense. Within a relatively short period of time, the tornado appeared to expand became centered within the low-level mesocyclone (Fig. 11b). In addition, it appeared to have a two-cell multiple-vortex structure. The tornado was traveling to the northeast at $\sim 15 \text{ m s}^{-1}$ (Figs. 10a and

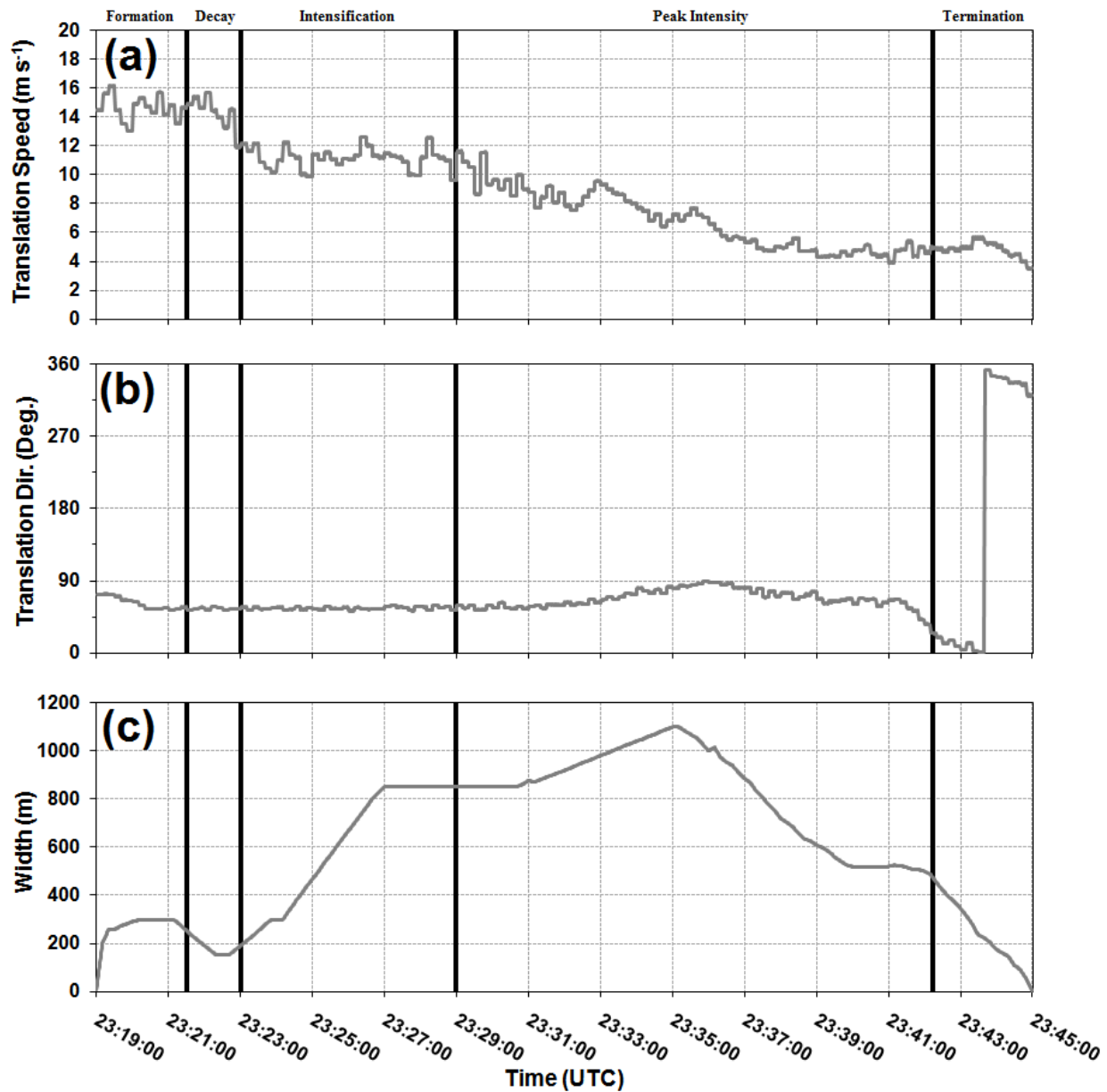


Figure 10. Temporal evolution of the Bowdle tornado's a) translation speed, b) translation direction, and c) width. Vertical black bars correspond to the intensity periods (labeled at the top) identified in Fig. 9.

10b). Only minor damage was observed at this time. Power poles paralleling Highway 47 were snapped at the base, and were given an EF-1 rating by the ABR NWS (Fig. 9).

During this period, the mesonet stations were in the process of repositioning from an earlier deployment on tornado episode #1 (see Finely et al. (2010)). Stations M1, M2, and M3 were well west of the tornado and traveling east along Highway 12. MT was already northeast of the tornado on Highway 12, preparing for a deployment of in situ instrumentation. Given the mesonet stations' tornado-relative positioning at this time, no close proximity measurements were obtained during this period.

3.2.2 Decay: 2321:30 - 2323:00

At approximately 2321:30, the occupants in MT observed a rapid decrease in tornado intensity that lasted until approximately 2323:00. Although the condensation funnel lifted from the ground during this period, a ground circulation, estimated to be approximately 200 m in diameter (Fig. 10c), was still visibly evident beneath a broader funnel aloft. Occupants in MT noted strong rotation within the mesocyclone during this period. The tornado slowed down slightly to $\sim 12 \text{ m s}^{-1}$ by the end of the period.



Figure 11. Video screenshots of the Bowdle tornado taken at the beginning of the a) formation, b) decay, c) intensification, d) peak intensity, and e) decay/termination periods during the tornado's life. Panel f) shows the Bowdle tornado approximately 50 seconds prior to termination. All times are in UTC. Panels a) and b) are courtesy of Skip Talbot.

Mesonet stations M1, M2, and M3 were still well west of the tornado during this period and were not within the 1 km distance-to-tornado-edge threshold for this study yet. MT was positioned northeast of the tornado, and the occupants were in the process of making a deployment of in situ instrumentation. However, the edge of the tornado was also in excess of 1 km from MT during this period as well.

3.2.3 Intensification: 2323:00 - 2329:00

At approximately 2323:00, the tornado began showing signs of re-intensifying. At the beginning of this period, M1 was approaching the tornado from west on Highway 12, and the tornado became visible at this time. Strong rotation was observed in the mesocyclone from M1's position. The condensation funnel was positioned above a broad, re-intensifying, multiple-vortex ground circulation beneath it (Fig 11c). The

tornado maintained a near-constant translation speed of $\sim 11 \text{ m s}^{-1}$ while traveling northeast (Figs. 10a and 10b).

As the Bowdle tornado crossed Highway 12, a large farmstead was in its path. Damage to this farm was rated EF-2 by the ABR NWS. Situated to the east of the farm was an instrument deployed by MT for making in situ measurements in and near a tornado. Preliminary analysis of video and damage in this area suggests the instrument sampled the eastern edge of the tornado. An analysis of these measurements is planned at a later time.

After the tornado struck the farmstead near Highway 12, it continued to move northeast into open terrain and substantially widen. Several large multiple-vortex structures were evident in the tornadic circulation as well. Based on a damage survey the following day, the tornado appeared to reach a width of $\sim 750 \text{ m}$ toward the end of this period (Fig 10c).

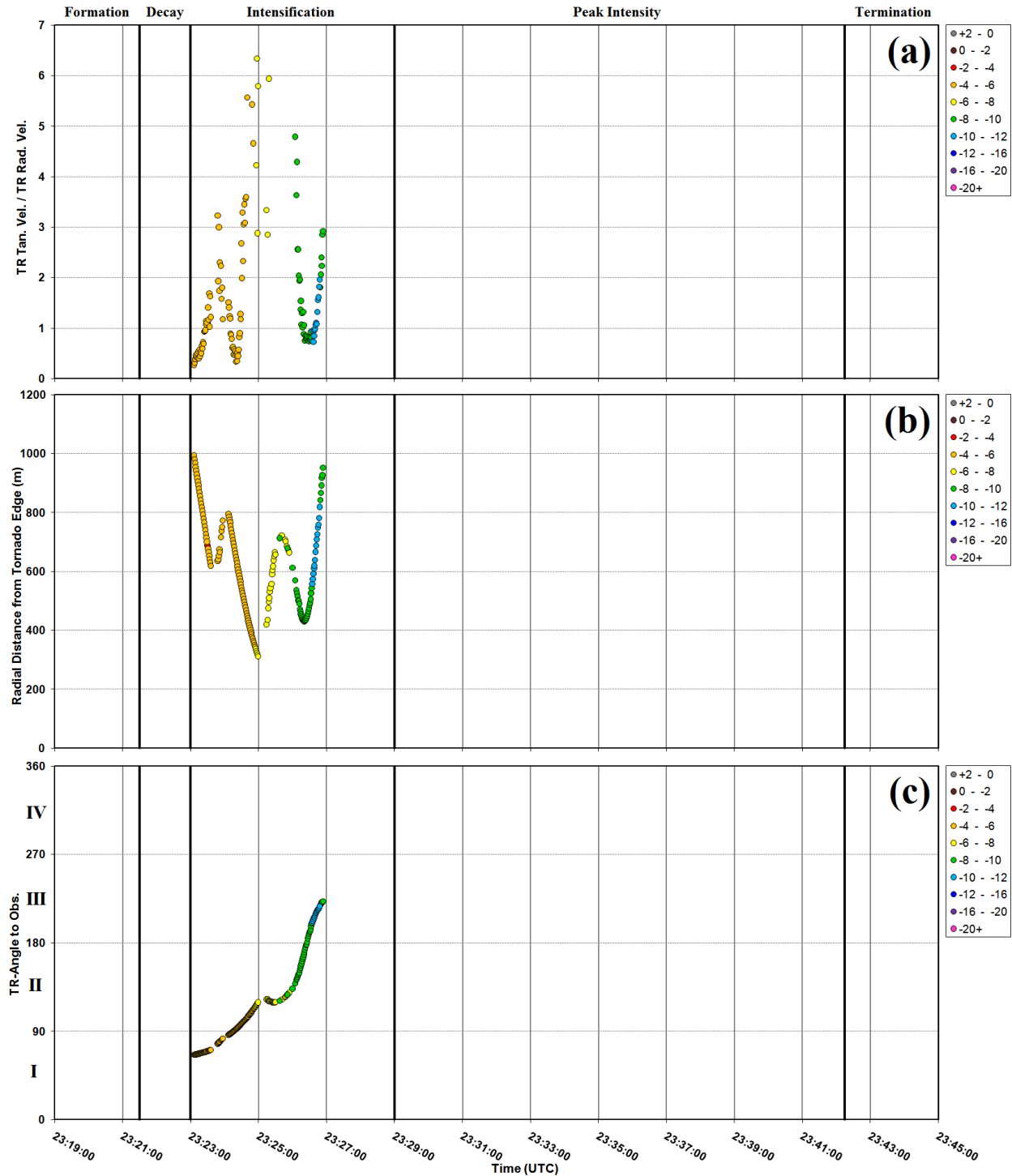


Figure 12. As in Fig. 7, except for the Bowdle Tornado.

As the tornado drew closer to MT, located northeast of the tornado initially, several observations were obtained meeting our distance criteria. The tornado passed by MT to the west and north, thus close proximity measurements were obtained within quadrants I, II and III (Fig. 12c). The flow with the largest radial components was measured east and east-

southeast of the tornado, with S_i values near zero (i.e. almost completely radial flow; Fig. 12a). These air parcels had θ_e deficits ranging from -4 to -6 K and θ_v deficits from 0 to -1 K (Figs. 12 and 13). As the tornado passed by to the west, northwest, north, and eventually north-northeast, the flow showed larger tangential components, especially

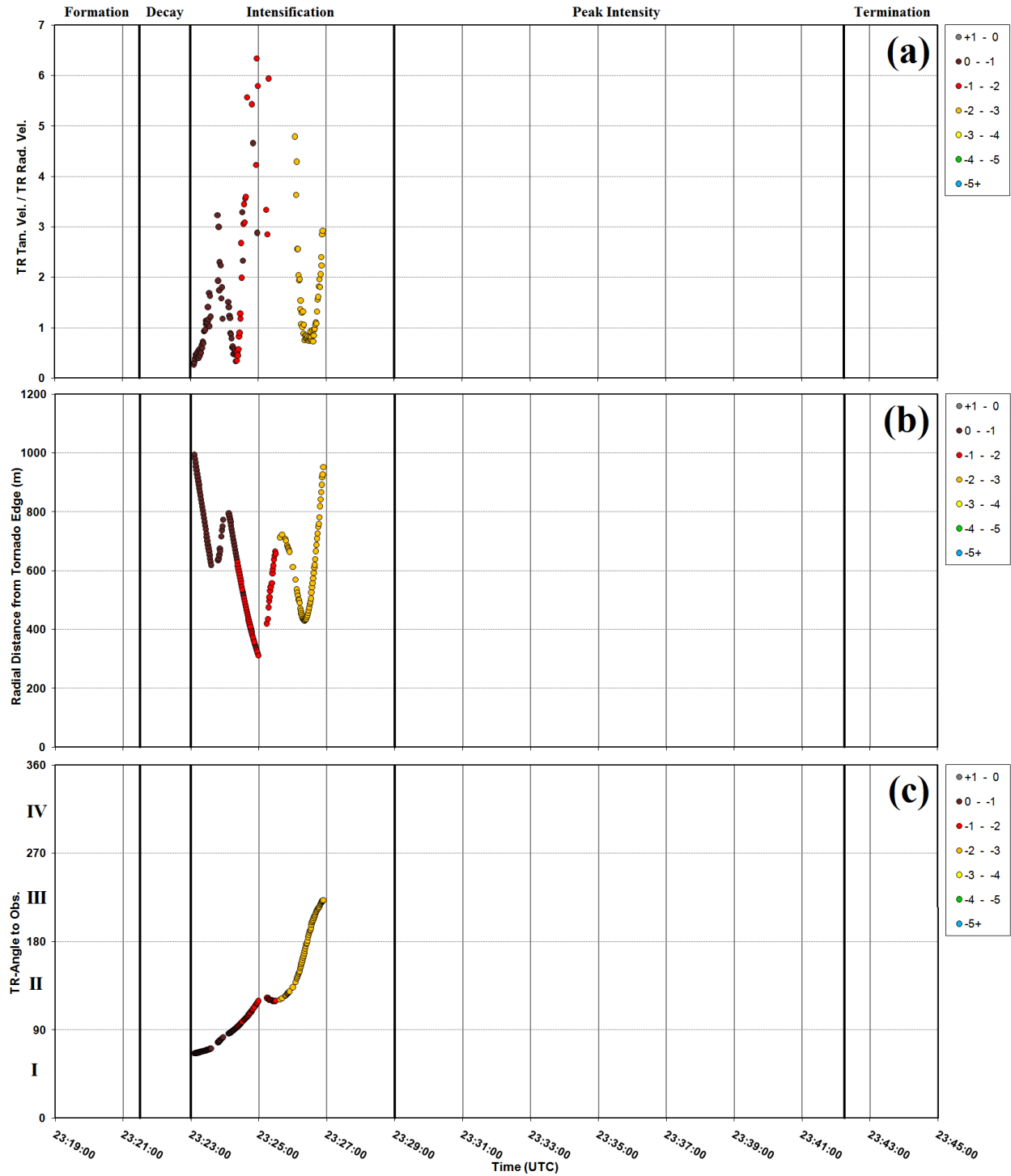


Figure 13. As in Fig. 12, except for θ_v' .

with increasing distance from the tornado edge. Additionally, the θ_e and θ_v deficits grew slightly larger, into the -8 to -10 K and -2 to -3 K range, respectively. As in the Aurora case, the θ_v deficits are generally consistent with the general hypothesis from Markowski et al. (2002) and Grzych et al. (2007). However, the θ_e deficits were comparatively large to these previous

studies, but still smaller than deficits from the Aurora case.

3.2.4 Peak Intensity: 2329:00 - 2342:15

The Bowdle tornado visually appeared to reach peak intensity at approximately 2329:00 (Fig. 11d),

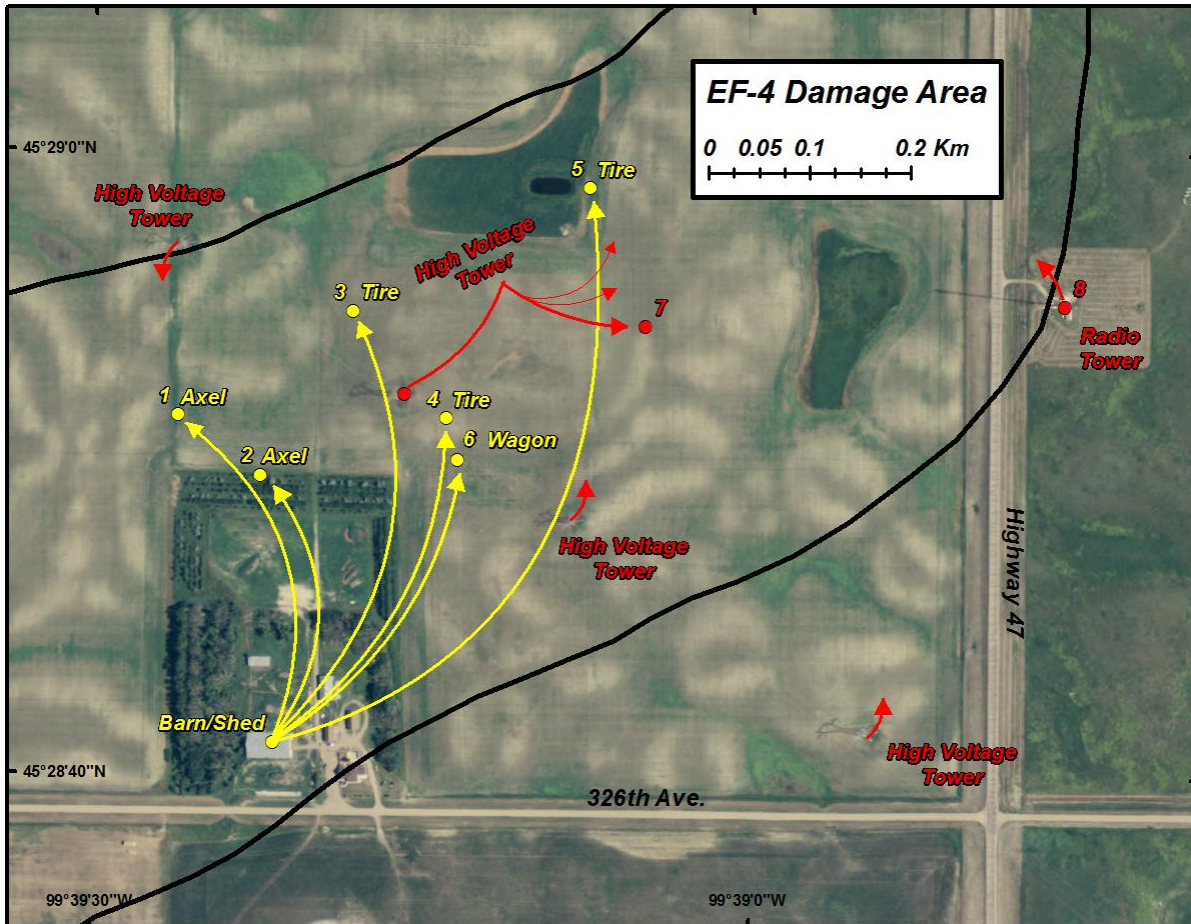


Figure 14. End locations of large objects that became airborne in the Bowdle tornado, relative to their origin. Arrows indicate direction of motion and/or directional orientation. Numbers correspond to the items listed in Table 1.

lasting several minutes, until about 2342:15. During this period of time, the translation speed of the tornado markedly slowed, from $\sim 10 \text{ m s}^{-1}$ to $\sim 5 \text{ m s}^{-1}$ (Fig. 10a), while its translation direction changed to nearly due east (Figs. 9 and 10b). The tornado also widened, followed by steady contraction in width through the remainder of this period, while maintaining its intensity with an apparent two-cell structure (Fig. 10c). Based on a post-event damage survey, we determined the maximum width to be approximately 1100 meters. This estimation is consistent with the ABR NWS determination of maximum tornado width (NCDC 2010). As evident on Fig. 9, the maximum size occurred northwest of Bowdle in mostly open farm fields. The most intense scouring along the tornado path was evident in this location, with fields reduced to bare dirt and gravel on the roads completely removed.

Two farmsteads were caught on the edge of the tornado during the middle part of this period. EF-1 damage was observed to a few grain bins on the northwest side of the tornado, and an agricultural building on the tornado's south side incurred EF-3 damage.

Near the end of this period, the southern half of the tornado passed through yet another farmstead. Given the availability of more damage indicators in this area, including several large objects, damage in this area was much more intense. In our post-event damage survey, a handheld GPS device was used to obtain geospatial coordinates of several large objects that were observed in the area near the farm (Figs. 14, 15, and Table 1). Critical information regarding the origins of these objects was provided by the farm owner's son (personal communication, C. Rieger 2010). An estimate of the distance each object traveled is also provided in Table 1. It is important to note that these distances are to be considered minimum distances. In all likelihood, these objects took a more curved path to their destination.

Objects originating from the shed west of the house traveled relatively large distances (Fig 14), including a tractor tire that flew at least 600 m. As evident on Figures 14 and 15, the southern side of the tornado (i.e., corner flow region) passed over this shed. Interestingly, numerical simulations of translating vortices have shown that flow on this side of the tornado, where the tornado's

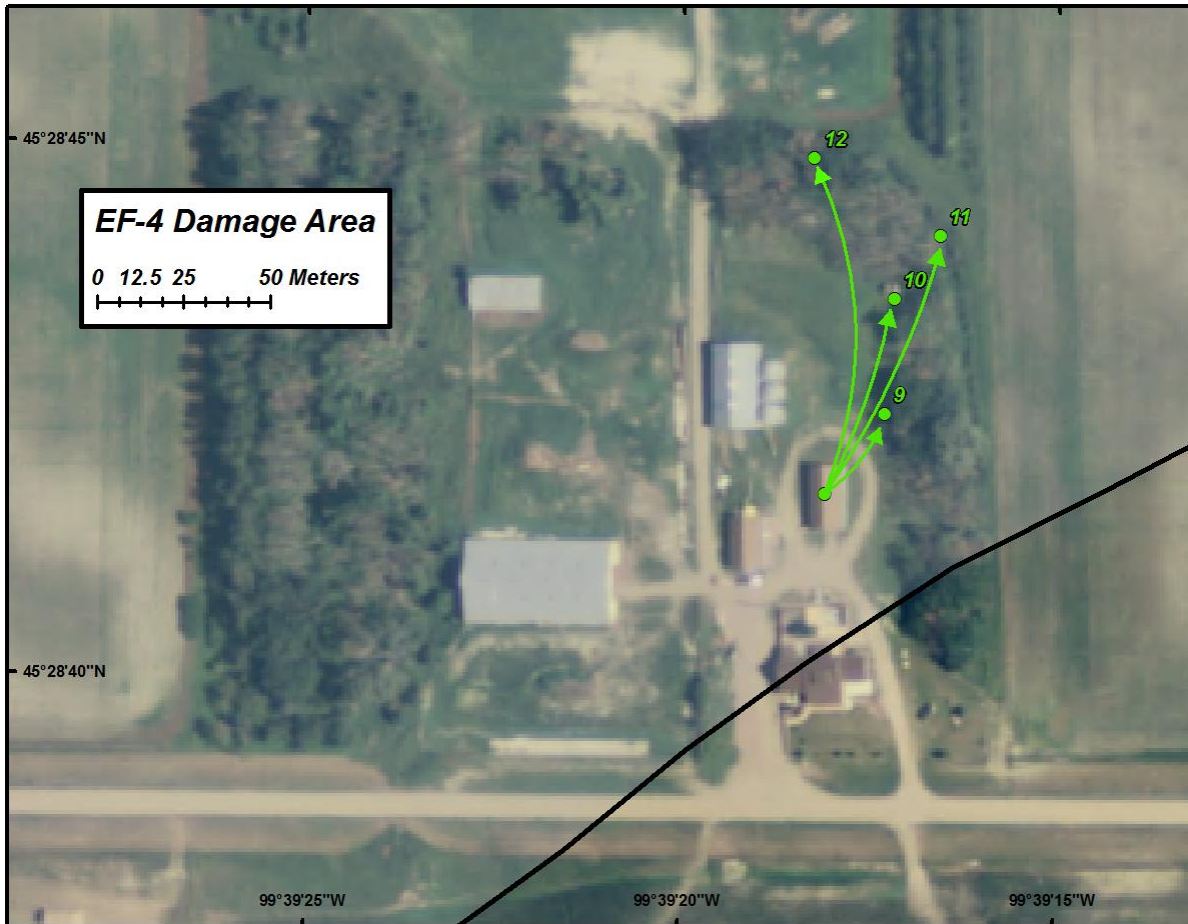


Figure 15. As in Fig. 14.

translation vector and an air parcel's velocity vector are aligned (e.g., Lewellen et al 2000), tends to have larger angular momentum. However, it is unknown whether this may have played a role in enhancing the damage that was observed in this region. Very little of this shed and structures nearby remained.

In addition to large objects thrown from the shed, three SUVs and one pickup truck were removed from a garage behind the house (Fig. 15). One of these vehicles, a white SUV, became airborne and landed in a shelterbelt to the north of the house. This vehicle traveled an estimated 100 m. The garage structure and all of its contents were completely swept clean from the concrete slab.

After leaving the farmstead, the tornado passed through a line of high-voltage transmission towers that were connected by several, approximately 3 inch diameter, power cables. As is evident in Fig. 14, towers southeast of the tornado fell toward the northeast, and towers to the northwest fell toward the southwest (several not shown in Fig. 14). Two towers were caught inside the tornado. One of these towers was located on the tornado's southern side, and this structure had two of its legs snapped from their concrete base, with the remaining two legs still attached. The other tower,













located more in the center of the tornado track, had all four of its legs sheared off at the base. This tower traveled northeast up and over a hill, while scouring out large sections of sod, in some places estimated to be 1.5 ft deep. Based on the scouring evidence, the tower made an abrupt turn toward the southeast. At this time, we believe the tower made a cusplike pattern in the sod, as evidenced in Figure 14. Note that the smaller red arrows in Figure 14 denote where pieces of this metal structure ended up. This tower and the other large objects listed in Table 1 represent the higher-end damage that was observed from this tornado, and an EF-4 rating was assigned to it by the ABR NWS.

Given the extreme danger of positioning teams to within 1 km of the edge of the tornado during this period, no measurements were obtained that met our distance threshold for this study.

3.2.4 Decay/Termination: 2342:15 - 2345:00

As the Bowdle tornado approached Highway 47 from the west, the tornado appeared to slow down and become almost stationary, as viewed from the south. However, based on video documentation and personal communication with a storm chaser positioned north of

Table 1. Estimated linear distances traveled by the objects labeled on Figs. 14 and 15.

Object Number	Object	Distance Traveled (m)	Picture	Object Number	Object	Distance Traveled (m)	Picture
1	Semi Trailer Axel	337		7	High Voltage Transmission Tower	250	
2	Semi Trailer Axel	265		8	South Dakota State Radio Tower	0 (Fell)	
3	Tractor Tire	436		9	Ford Excursion	27	
4	Tractor Tire	365		10	Ford Expedition	59	
5	Tractor Tire	632		11	Ford F-250	81	
6	Gravity-Flow Grain Wagon	335		12	Toyota Hilander	100	

the tornado during this period (A. Gabrielson, 2010), we believe the tornado moved north, paralleling Highway 47, before terminating in the field west of the highway at approximately 2345:00 (Figs. 10, 11e, and 11f).

As the southeastern edge of the tornado crossed Highway 47, it came very close to a large metal radio tower, located on the east side of the highway (Fig. 9). This structure failed, but did not leave the site. Damage here was assigned an EF-2 rating.

The tornado was not visible from the south for the last 50 seconds of this period because the Bowdle storm was quickly transitioning toward a high-precipitation supercellular structure. Loss of visibility and the termination of the tornado was thought to be the result of a cell merging process, with convection that developed south of the storm. Given the lack of visibility at this time, no measurements in close proximity to the tornado were obtained.

4. PRELIMINARY CONCLUSIONS

The temporal evolution of tornado track, intensity, and structure from two significantly tornadic events, the Aurora tornado and the Bowdle tornado, have been documented in this study. Aerial orthophotos taken shortly after the Aurora tornado allowed for a unique way of digitizing the tornado track, and we are hopeful this can be done for the Bowdle tornado as well. Mobile mesonet wind measurements made within 1 km of the edge of both tornadoes were decomposed into their radial and tangential velocity components, and the evolution of these components was compared to the evolution of the tornadoes. Additionally, the thermodynamic properties of these close proximity observations were also compared to the evolution of the tornado.

We have shown that the near-ground winds near a tornado are highly asymmetric in both time and space. It appears there may be some linkage between S_i , θ_e , and θ_v and tornado intensity and structure, however, the results we've obtained thus far are very preliminary and far from complete given the non-uniform population of the four quadrants. Large radial wind components ($0 < S_i < 1$) were generally observed just prior to or during tornado intensification, with limited support from visual evidence of the tornado indicating a lower-swirl corner flow structure. Unfortunately, few observations were obtained during the decay period(s) of both tornadoes. Thus, we can only offer a limited amount of information about the nature of the flow and how it could be affecting the intensity of the tornado during its demise.

Thermodynamically, the environment in close proximity to a tornado also appears to be quite inhomogeneous in time and space. In general, relatively small θ_e deficits were observed during periods of intensification, with larger deficits occurring shortly before or shortly after periods of decay, but not in all instances. These more (less) thermodynamically favorable parcels were found to be associated with flow that had larger radial wind components shortly before or during tornado intensification (decay). Finally, θ_v deficits were found to be generally consistent with the findings

of Markowski et al. (2002) and Grzych et al. (2007), however, θ_e deficits were found to be comparatively large for these significant tornadic events.

Of course, a substantial shortcoming to this study is a lack of close proximity, quasi-concurrent near-ground measurements in all quadrants. Given the limited measurements from only two tornadoes have been analyzed thus far, these results are very preliminary. Obviously, the logistics in obtaining a dataset sufficient for the goals of this work are nearly impossible. However, we believe some headway can still be made. It seems the most appropriate strategy would be to deploy several in situ instruments in a dense, spatial array, with supplementary information provided by mobile mesonet stations. This type of dataset could provide at least a snapshot of the flow and its thermodynamic properties at a particular stage in a tornado's life.

5. FUTURE WORK

This study, as it currently stands, presents close proximity measurements from only two cases. We hope to include measurements from at least three additional cases, including 29 May 2008 near Tipton, KS, 5 June 2009 near LaGrange, WY, and 13 June 2010 near Booker, TX. Additional cases from the 2009 and 2010 severe storms seasons are also being analyzed for potential inclusion into this study. Further, in situ measurements obtained from the 22 May 2010 and 17 June 2009 cases are planned for inclusion into this study at a later time.

We are hopeful to improve upon our assessment of the Bowdle tornado track, by obtaining orthophoto imagery from the 2010 National Agriculture Imagery Program (NAIP). While conducting our damage survey of the Bowdle tornado, it became apparent that obtaining GPS waypoints of scouring produced by the tornado, in addition to waypoints for damage, would be highly valuable to future research efforts. We plan to incorporate the use of GPS in a more substantial way in future damage surveys.

6. ACKNOWLEDGEMENTS

Partial support for the research was provided by NOAA grants NA06OAR4600230, NA08OAR4600887, and NA09OAR4600222, and by the National Geographic Society and the Discovery Channel. We thank all past participants of TWISTEX for volunteering their time and effort toward this project. We thank Ryan Pfannkuch, Jeremy Wesely, Rick Ewald, Steve Kisner, and Scott Bryant of the NWS Hastings, NE for sharing pictures and information related to their damage assessment of the 17 June 2009 tornadoes. We especially thank Jim Scarlett, Dave Hintz, and Mike Fowle of the NWS Aberdeen, SD for their correspondence and sharing of aerial photos from the 22 May 2010 event. We thank Gayle Follmer and the Nebraska DNR for providing high-resolution quadrangle aerial orthophotos and metadata used to digitize the tornado track of the 17 June 2009 tornado. We also

thank Andy Gabrielson and Skip Talbot for sharing video documentation of the 22 May 2010 event.

7. REFERENCES

- Brown, J. M., and K. R. Knupp, 1980: The Iowa cyclonic-anticyclonic tornado pair and its parent thunderstorm. *Mon. Wea. Rev.*, **108**, 1626–1646.
- Church, C. R., J. T. Snow, G. L. Baker and E. M. Agee, 1979: Characteristics of tornado-like vortices as a function of swirl ratio: A laboratory investigation. *J. Atmos. Sci.*, **36**, 1755–1766.
- Doswell, C. A., III, H. E. Brooks, and N. Dotzek, 2009: On the implementation of the Enhanced Fujita scale in the USA. *Atmos. Res.*, **93**, 554–563.
- Finley, C. A., B. D. Lee, M. Grzych, C. D. Karstens, and T. M. Samaras, 2010: Mobile mesonet observations of the rear-flank downdraft evolution associated with a violent tornado near Bowdle, SD on 22 May 2010. Preprints, *25th Conf. on Severe and Local Storms*, Denver, CO, Amer. Meteor. Soc., paper 8A.2.
- Golden, J. H., and D. Purcell, 1977: Photogrammetric velocities for the Great Bend, Kansas tornado of 30 August 1974: Accelerations and asymmetries. *Mon. Wea. Rev.*, **105**, 485–492.
- Grzych, M. L., B. D. Lee, and C. A. Finley, 2007: Thermodynamic analysis of supercell rear-flank downdrafts from Project ANSWERS. *Mon. Wea. Rev.*, **135**, 240–246.
- Hirth, B. D., J. L. Schroeder, and C. C. Weiss, 2008: Surface analysis of the rear-flank downdraft outflow in two tornadic supercells. *Mon. Wea. Rev.*, **136**, 2344–2363.
- Karstens, C. D., T. M. Samaras, B. D. Lee, W. A. Gallus, Jr., and C. A. Finley, 2010: Near-ground pressure and wind measurements in tornadoes. *Mon. Wea. Rev.*, **138**, 2570–2588.
- Kosiba, K. A., R. J. Trapp, and J. Wurman, 2008: An analysis of the axisymmetric three-dimensional low level wind field in a tornado using mobile radar observations. *Geophysical Research Letters*, **35**, L05805.
- Lee, B. D., C. A. Finley, and T. M. Samaras, 2010a: Surface Analysis Near and Within the Tipton, Kansas Tornado on 29 May 2008. *Mon. Wea. Rev.*, in press.
- , ———, C. D. Karstens, and T. M. Samaras, 2010b: Surface observations of the rear-flank downdraft evolution associated with the Aurora, NE tornado of 17 June 2009. Preprints, *25th Conf. on Severe and Local Storms*, Denver, CO, Amer. Meteor. Soc., paper P8.27.
- Lewellen, W. S., D. C. Lewellen, and J. Xia, 2000: The influence of a local swirl ratio on tornado intensification near the surface. *J. Atmos. Sci.*, **57**, 527–544.
- Markowski, P. M., J. M. Straka, and E. N. Rasmussen, 2002: Direct surface thermodynamic observations within the rear-flank downdrafts of nontornadic and tornadic supercells. *Mon. Wea. Rev.*, **130**, 1692–1721.
- NCDC, 2010: Storm Data. Vol. 52, No. 5, 147 pp. [Available from National Climatic Data Center, 151 Patton Ave., Asheville, NC 28801.]
- NWS, cited 2010a: EF1 tornado north of Gibbon June 17. [Available online at http://www.crh.noaa.gov/news/display_cmsstory.php?wfo=gid&storyid=28857&source=2.]
- NWS, cited 2010b: Weak tornado passes through southern Grand Island on June 17th. [Available online at http://www.crh.noaa.gov/news/display_cmsstory.php?wfo=gid&storyid=28945&source=2.]
- NWS, cited 2010c: EF2 tornado west of Aurora June 17. [Available online at http://www.crh.noaa.gov/news/display_cmsstory.php?wfo=gid&storyid=28856&source=2.]
- Snow, J. T., C. R. Church, and B. J. Barnhart, 1980: An investigation of the surface pressure fields beneath simulated tornado cyclones. *J. Atmos. Sci.*, **37**, 1013–1026.
- Straka, J. M., E. N. Rasmussen, and S. E. Fredrickson, 1996: A mobile mesonet for finescale meteorological observations. *J. Atmos. Oceanic Technol.*, **13**, 921–936.
- Wakimoto, R. M., H. V. Murphey, D. C. Dowell, and H. B. Bluestein, 2003: The Kellerville tornado during VORTEX: Damage survey and Doppler radar analysis. *Mon. Wea. Rev.*, **131**, 2197–2221.